Anti-tumor activity of paclitaxel through dual-targeting carrier of cyclic RGD and transferrin conjugated hyperbranched copolymer nanoparticles

Qing Xu [a], Yuexian Liu [a], Shishuai Su [a], Wei Li [b], Chunying Chen [a,*], Yan Wu [a,**]

[a] CAS Key Lab for Biomedical Effects of Nanomaterials and Nanosafety, National Center for Nanoscience and Technology, Beijing 100190, China
[b] Institute of High Energy Physics, Chinese Academy of Sciences, Beijing 100049, China

ABSTRACT

Targeted delivery strategies are becoming increasingly important. Herein, a novel hyperbranched amphiphilic poly[(amine-ester)-co-(D,L-lactide)]/1,2-dipalmitoyl-sn-glycero-3-phosphoethanolamine copolymer (HPAE-co-PLA/DPPE) with RGD peptide (cRGDfK) and transferrin (Tf) on the periphery was synthesized and used to prepare paclitaxel-loaded nanoparticles (NPs) for dual-targeting chemotherapy. These NPs show satisfactory size distribution, high encapsulated efficiency and a pH-dependent release profile. The intrinsic fluorescence of the hyperbranched copolymer renders the detection and tracking of NPs *in vitro* and *in vivo* conveniently. *In vitro* cytotoxicity studies proved that the presence of cRGDfK enhanced the cytotoxic efficiency by 10 folds in $\alpha_v\beta_3$ integrin over-expressed human umbilical vein endothelial cells, while Tf improved cytotoxicity by 2 folds in Tf receptor over-expressed human cervical carcinoma cells. The drug-loaded NPs can be efficiently transported into the vascular endothelial cells and the target tumor cells. These results indicate that the cRGDfK and Tf decorated HPAE-co-PLA/DPPE could deliver chemotherapies specifically inside the cell via receptor-mediated endocytosis with greater efficacy. Therefore, such a fluorescent nanocarrier prepared from non-cytotoxic and biodegradable polymers is promising for drug delivery in tumor therapy.

1. Introduction

Chemotherapy is essential in the treatment of malignant tumors, however, its efficacy is usually limited due to the poor physiochemical properties, low stability, short circulating half-life, and the toxicity to normal tissues associated with the anti-tumor drugs. Paclitaxel (PTX), a major chemotherapeutic drug extracted from the bark of *Taxus brevifolia*, is widely used to treat patients with lung, ovarian, breast cancer and advanced forms of Kaposi's sarcoma [1,2]. However, its high hydrophobicity and serious side effects greatly limit its clinical application [3]. Drug delivery systems have been investigated for many years and among them, encapsulating drugs into the hydrophobic core of self-assembled polymer micelles in an appropriate size range is a promising alternative. Polymeric micelles are thermodynamically stable, and the hydrophilic shell enhances its stable dispersion in aqueous solution by a steric stabilization effect, which assists its long-term

blood duration following intravenous injection [4]. Moreover, polymeric nanoparticles (NPs) can target tumors by either a passive or active process. Passive targeting indicates that NPs can enter the leaky endothelial tissue that surrounds the tumor and accumulate in certain solid tumors by the well-known enhanced permeation and retention (EPR) effect [5]. Active targeting is delivering drugs to a specific site in terms of molecular recognition with a suitable ligand which can recognize its receptor on the targeting site [6]. Among all the neoplastic targeting ligands that are presently under investigation, the RGD sequence and transferrin (Tf) are two popular ones used in drug delivery systems [6].

The RGD sequence, an arginine-glycine-aspartic acid (RGD) tripeptide, has been proved to be an efficient binding motif to assist interactions between drug delivery systems including NPs and some integrins which mediate binding between cells and proteins of the extracellular matrix [7]. Among these integrins, integrin $\alpha_v\beta_3$ was proved to be over-expressed on the angiogenic endothelium in malignant or diseased tissues [8]. Histological analysis of breast cancer biopsy tissue also exhibited that $\alpha_v\beta_3$ was an important marker of blood vessels in the most malignant tumors, making it an attractive target for anti-angiogenesis strategy [9–11]. Various peptides containing RGD sequence have been developed to be ligands of $\alpha_v\beta_3$ integrin for therapeutical applications. cRGDfK

* Corresponding author. National Center for Nanoscience and Technology of China, Beijing 100190, China. Tel.: +86 10 82545560; fax: +86 10 62656765.
** Corresponding author. Tel.: +86 10 82545614; fax: +86 10 62656765.
E-mail addresses: chenchy@nanoctr.cn, chenchy@ihep.ac.cn (C. Chen), wuy@nanoctr.cn (Y. Wu).

peptide, cyclic (arginine-glycine-aspartic acid-phenylalanine-lysine), is usually chosen as it can alternatively bind to the $\alpha_v\beta_3$ integrin receptors with high affinity [12].

Transferrin (Tf) is a human serum glycoprotein ($\sim$80 kDa) involved in the delivery of ferric ions throughout the body. Tf is transported into cells through a receptor-mediated endocytosis via the transferrin receptor (TfR) [13]. Many studies have indicated that the expression level of TfR on tumor cells is much higher than that on normal cells [14,15], which has been widely utilized for targeting drug delivery systems as a novel potential approach [6,16,17].

Versatile polymeric vehicles have been widely used for drug delivery. Dendritic polymers, including dendrimers and hyperbranched polymers, have a highly branched structure, intra-molecular voids, small rheological volumes and lower viscosity in solution, providing a high density of functional groups at the periphery [18,19]. Previously we first synthesized a series of amphiphilic hyperbranched poly[(amine-ester)-co-(D,L-lactide)] (HPAE-co-PLA) and HPAE-co-PLA/DPPE copolymers that were used as carriers for both hydrophilic and hydrophobic drugs, achieving improved water solubility, high entrapment efficiency and controlled release in vitro [20,21]. As DPPE is a phospholipid with both high biocompatibility and high flexibility in the lipid bialyer of cell membrane, the HPAE-co-PLA/DPPE copolymers show better absorbability than HPAE-co-PLA [21–23].

In present work, we aim to construct a dual-targeting PTX-loaded NPs based on HPAE-co-PLA/DPPE copolymer, which was modified with two targeting ligands, RGDfK and Tf. RGDfK has high affinity with the $\alpha_v\beta_3$ integrin, which is a primary marker of tumor vessels and Tf is specific ligand for TfR, which is over-expressed on tumor cells. Thus, these dual-targeting NPs may achieve more accumulation and improved lethality of the PTX-loaded NPs in tumors (Scheme 1C). Passive targeting is achieved by extravasation of NPs through enhanced permeability of the tumor vasculature. Active tumors targeting can be achieved in two steps: the ligand RGD enhances the targeting migration and accumulation of NPs to the $\alpha_v\beta_3$ integrin-expressing tumor vasculature and Tf then improves the cellular uptake of NPs by TfR-expressing tumor cells. In addition, a heterobifunctional cross-linker, p-maleimidophenyl isocyanate (PMPI), used for hydroxyl to sulfhydryl coupling should be introduced to the HPAE-co-PLA/DPPE copolymer for the successful modification of targeting ligands [24,25].

In present paper, we firstly constructed the PMPI-HPAE-co-PLA/DPPE copolymer, and then two target ligands, RGDfK and Tf, were linked to form the tumor-targeting drug nanocarrier. NPs loaded with PTX were prepared by the emulsion/solvent evaporation method and characterized for surface morphology, size distribution, drug encapsulation efficiency, and in vitro release. Finally, the cytotoxicity and cellular uptake of PTX-loaded NPs against human umbilical vein endothelial cells (HUVECs) and human cervical carcinoma (HeLa) cells were evaluated for their tumor-targeting effects using the CCK-8 assay, confocal laser scanning microscopy (CLSM), and flow cytometry.

2. Materials and methods

2.1. Materials

1, 1, 1-Trimethylolpropane and methyl acrylate purified by vacuum distillation and diethanolamine were purchased from National Medicines Chemical Reagent Co. Ltd (Shanghai, China). Titanium tetraisopropoxide (Ti(OiPr)$_4$), benzoic anhydride and imidazole were purchased from Beijing Reagent Factory (Beijing, China). D, L-Lactide (DLLA), Transferrin (Tf), 2-iminothiolane hydrochloride (Traut's reagent), 5, 5-Dithiobis (2-nitrobenzoic acid) (Ellmann's reagent) was obtained from Alfa Aesar (Ward Hill, MA, USA). 1,2-dipalmitoyl-sn-glycero-3-phosphoethanolamine (DPPE) was purchased from Avanti Polar Lipids, Inc (Alabaster, Alabama, USA). Sn(Oct)$_2$, 4-nitrophenyl chloroformate (pNP) (97%), 4-dimethylaminopyridine (DMAP) (99%), p-maleimidophenyl isocyanate (PMPI) and dibutylin dilaurate (DBTDL) were

purchased from Sigma–Aldrich (St. Louis, MO, USA). Paclitaxel (PTX) was purchased from Beijing HuaFeng Unite Co, Ltd (Beijing, China). Commercial Cell Counting-8 (CCK-8) Kits were purchased from Dojindo Laboratories (Japan). RGDfK-SH was purchased from ChinaPeptides Co, Ltd (Shanghai, China). All other reagents and solvents were of analytical grade.

Human Umbilical Vein Endothelial cells (HUVECs) and human cervical carcinoma (HeLa) cells were purchased from American Type Culture Collection (ATCC; Manassas, VA, USA). Cells were cultured at 37 °C in a 5% CO$_2$ atmosphere in Dulbecco's modified Eagle's medium (DMEM, Gibco) supplemented with 10% fetal bovine serum (FBS, Gibco), penicillin (100 U/mL) and streptomycin (100 U/mL).

2.2. Synthesis and characterization of dual-targeting and fluorescent copolymers

The fluorescent PMPI-HPAE polymer was firstly obtained by reacting partial surface hydroxyl groups of HPAE (G4) with isocyanate groups from PMPI, a hetero-bifunctional cross-linker used for hydroxyl to sulfhydryl coupling. Then, PMPI-HPAE-co-PLA copolymers were prepared with a ring-opening polymerization method. The PMPI-HPAE-co-PLA/DPPE copolymers were afterward synthesized by the reaction of activated PMPI-HPAE-co-PLA-pNP and DPPE. Finally, the targeting copolymers were obtained by conjugating either Tf or RGDfK to the PMPI-HPAE-co-PLA/DPPE copolymers (Scheme 1A).

2.2.1. Synthesis of fluorescent PMPI-HPAE-co-PLA/DPPE copolymers

Hyper-branched poly(amine-ester) polymers (HPAE-OHs) were synthesized at 120 °C by alcoholysis through a pseudo-one-step process using 1,1,1-trimethylol propane (as a molecular core) and N,N-diethylol-3-amine methylpropionate (as an AB$_2$ monomer) with Ti(OiPr)$_4$ as the catalyst, according to our previous study [20,26]. The generation of HPAE-OHs was increased by repeatedly adding N,N-diethylol-3-amine methylpropionate monomer to the former reaction product. The fourth-generation product (i.e. HPAE-OHs4) was prepared by repeating the process three times.

The PMPI-HPAE polymer was synthesized by reacting partial surface hydroxyl groups of HPAE-OHs4 with isocyanate groups of PMPI [25]. Briefly, 500 mg of HPAE-OHs4 was dissolved in 4 mL dimethyl sulfoxide (DMSO), then 40 μL DBTDL and 400 μL triethylamine (TEA) were added. 20 mg of PMPI was dissolved in 1 mL DMSO and added to the HPAE-OHs4 solution. The mixture was stirred at 45 °C, under nitrogen flow, in darkness for 24 h. The obtained solution was precipitated in 150 mL cold ethyl acetate (EA), washed further with EA three times to remove the residual DMSO and catalyst, and dried at room temperature in a vacuum oven, and stored at −20 °C.

PMPI-HPAE-co-PLA copolymer at a molar ratio of 4:1 (DLLA/PMPI-HPAE-OHs4) was synthesized as previously described [26]. DLLA and PMPI-HPAE-OHs4 were put into a flask and Sn(Oct)$_2$ was added at about 0.1% (w/w). After 1 h of evacuation by a vacuum pump at 30 °C, the flask was sealed and heated to 140 °C in an oil bath. 13 h later, the reaction solution was cooled down to room temperature. The obtained viscous product was dissolved in methylene chloride (DCM) and precipitated with petroleum, and further washed three times with petroleum. After that, the petroleum was evaporated and the product was then dissolved in acetone and precipitated with deionized water. Finally, the purified PMPI-HPAE-co-PLA was dried in a vacuum oven at room temperature for 48 h.

PMPI-HPAE-co-PLA/DPPE copolymer was synthesized in two steps according to our previous study [20,27] with small changes. Firstly, the PMPI-HPAE-co-PLA was activated with pNP. 500 mg of PMPI-HPAE-co-PLA was dissolved in 5 mL chloroform by magnetic stirring and was pre-cooled in an ice bath for 20 min. 200 mg of pNP, 20 mg of DMAP and 0.5 mL pyridine were then added to the solution. The mixture was determined to react for 6 h at 0 °C and 10h at 25 °C under magnetic stirring. The obtained product was evaporated to partly remove the chloroform and precipitated with diethyl ether/petroleum ether (1:1, v/v). The precipitate was washed with the diethyl ether/petroleum ether for three times and dried in a vacuum oven at room temperature for 48 h. Secondly, PMPI-HPAE-co-PLA/DPPE copolymer was synthesized by reaction of DPPE and the above activation of PMPI-HPAE-co-PLA copolymer (PMPI-HPAE-co-PLA-pNP) with mass ratio of 1:15 (DPPE/PMPI-HPAE-co-PLA-pNP). The dehydrated PMPI-HPAE-co-PLA-pNP was dissolved in 5 mL chloroform and then DPPE solution containing 0.1 mol TEA was added dropwise. The reaction continued with magnetic stirring at room temperature under nitrogen in the absence of light for 24 h. After this time, the resulting product was evaporated to remove part of chloroform and precipitated with diethyl ether/petroleum ether (1:1, v/v). The precipitated PMPI-HPAE-co-PLA/DPPE was then washed three times with the diethyl ether/petroleum, dried in a vacuum oven at room temperature for 48 h and eventually stored at −20 °C as a powder.

The chemical structures of the polymers were detected with Fourier transform infrared spectroscopy (FT-IR) and nuclear magnetic resonance (NMR) spectral analysis. FT-IR spectra of the polymers were recorded on a spectrophotometer (Perkin–Elmer, Fremont, CA, USA) using KBr as a reference. ^{1}H NMR, ^{13}C NMR and ^{31}P NMR spectra of the polymers were obtained by a Bruker AVANCE 400 NMR spectrometer (Billerica, MA, USA). Molecular weight and molecular weight distribution were detected with permeation chromatography apparatus (Waters 2410, Milford, MA, USA). The fluorescence spectra of PMPI-HPAE-co-PLA/DPPE were detected by an LS 55 Fluorescence Spectrometer (Perkin–Elmer, Fremont, CA, USA)

A

PMPI-HPAE-co-PLA/DPPE   PMPI-HPAE-co-PLA/DPPE-RGD-Tf

B

HPAE-HOs4   PLA   DPPE   PTX   RGD   Tf

C

and the fluorescence quantum yield was determined with rhodamine B as a reference.

2.2.2. Synthesis of dual-targeting and fluorescent copolymers

Tf was first thiolated with Traut's reagent [28]. Briefly, 10 mg (0.12 μM) of Tf was dissolved in 2 mL 0.15 M Naborate buffer/0.1 mM EDTA (pH 8.5) and 0.7 mg (5.0 μM) of Traut's reagent was then added. After reaction under magnetic stirring at room temperature for 60 min, the mixture solution was replaced with 0.01 M HEPES (containing 0.01 mM EDTA and 0.15 M NaCl, pH 7.0) using Sartorius Stedim Vivaspin 6 centrifugal concentrator (MWCO 30 kDa). The extent of thiolation was determined using Ellman's reagent [29].

The targeting copolymers HPAE-co-PLA/DPPE-RGD, HPAE-co-PLA/DPPE-Tf, HPAE-co-PLA/DPPE-RGD/Tf obtained by modifying the PMPI-HPAE-co-PLA/DPPE copolymers with RGDfK-SH, Tf-SH or both of them, respectively, were prepared using the same procedure. Taking HPAE-co-PLA/DPPE-RGD/Tf as an example, 50 mg of PMPI-HPAE-co-PLA/DPPE copolymers were dissolved in 5 mL acetone and added to 10 mL deionized water dropwise under magnetic stirring. After 30 min, the reaction solution was evaporated under vacuum to remove acetone. The PMPI-HPAE-co-PLA/DPPE copolymers were collected by centrifugation at 13,000 rpm for 30 min at room temperature and resuspended in 5 mL 0.05M HEPES buffer (containing 0.01 M EDTA pH 6.5) [30]. 0.5 mg of cRGDfK was added and the mixture was stirred for 4 h at room temperature, then 10 mg of Tf-SH was added and the mixture was kept stirring for another 4 h [31]. Finally, the resulting product was centrifuged at 12,000 rpm for 6 min and washed with deionized water for three times to remove unreacted RGD-SH and Tf-SH.

2.3. Preparation of fluorescent PTX-loaded NPs

PTX containing polymeric NPs were prepared via an emulsion/solvent evaporation technique. Taking PTX-RGD/Tf-NPs as an instance, 10 mg of HPAE-co-PLA/DPPE-RGD/Tf copolymers were dissolved in 3 mL DCM and PTX were added with copolymer/PTX mass ratios of 5/1, 10/1, 50/1, 100/1. The mixture was slowly added to 10 mL an aqueous solution with 1–4% (w/v) of polyvinyl alcohol (PVA) and vigorously stirred at room temperature for 10 min. The mixture was then emulsified by sonication for 5 min at 40 w and evaporated under reduced pressure to remove the remaining methylene chloride. The NPs were recovered at room temperature by centrifugation at 12,000 rpm for 6 min and washed with deionized water for three times. Other PTX-loaded NPs (PTX-NPs, PTX-Tf-NPs, PTX-RGD-NPs) were made by the same procedure.

2.4. Loading content and encapsulation efficiency of PTX-loaded NPs

The drug loading content and encapsulation efficiency were determined by HPLC (Waters 2478, Milford, MA, USA) in triplicate with UV detection at 227 nm. A C18-column (Nova-Pak 3.9×250 mm, Waters, Milford, MA) was used with a mobile phase consisted of water and acetonitrile (20:80 v/v) and the flow rate was 1 mL/min. The lyophilized PTX-loaded NPs were also dissolved in acetonitrile. The loading content and encapsulation efficiency was defined as follows [32]:

$$\text{Loading content (\%)} = W_t/W_S \times 100\%$$

$$\text{Encapsulation efficiency (\%)} = W_t/W_0 \times 100\%$$

W_0 and W_t are the weight of initial PTX and PTX detected in the NPs. W_S is the weight of NPs after lyophilization.

2.5. Characterization

The average size, polydispersity index and zeta potential were determined by dynamic light scattering (DLS) using a ZetaSizer Nano series Nano-ZS (Malvern Instruments Ltd, Malvern, UK). Determinations were performed at 633 nm with a constant angle of 90° at 25 °C after samples were appropriately diluted in distilled water, PBS and DMEM (with 10% FBS), respectively.

The morphology of the NPs was observed by transmission electron microscopy (TEM) (EM-200CX; JEOL Ltd., Tokyo, Japan) following negative staining with uranyl acetate.

2.6. In vitro drug release

In vitro release of PTX from NPs was investigated by dialysis method. The freeze-dried PTX-loaded NPs were dispersed in 3 mL deionized water and then put into a dialysis bag (MWCO: 3000 Da). The end-sealed dialysis bag was incubated in 35 mL different mediums (phosphate buffer with pH 7.4 and 5.2 respectively) at 37 °C and shaken in the water bath at a speed of 110 rpm. 0.5 mL of supernatant were extracted at predetermined time intervals and replaced with 0.5 mL fresh PBS. The concentration of PTX released from NPs was determined by HPLC as described above.

2.7. Cytotoxicity assay

HUVECs and HeLa cells were seeded at a density of 5×10^3 cells per well in 96-well plates in DMEM medium and incubated for 24 h. The medium was then replaced with 200 μL of medium containing various equivalent concentrations of free-PTX, PTX-NPs, PTX-RGD-NPs, PTX-Tf-NPs and PTX-RGD-Tf-NPs. The cells were incubated for 24 h or 48 h and cytotoxicity was performed using CCK-8 Kits (Dojindo Molecular Technologies, Tokyo, Japan). Absorbance was detected at 450 nm with TECAN Infinite M200 microplate reader (Tecan, Durham, USA). Each experiment was repeated for three times.

2.8. Cellular uptake

To quantitatively measure the internalization of NPs, HUVECs and HeLa cells were incubated in 6-well plates for 24 h to about 80% confluence. NPs, RGD-NPs, Tf-NPs and RGD-Tf-NPs (concentration for PMPI-HPAE-co-PLA/DPPE copolymer in various NPs, 250 μg/mL) were then added to specified wells. After incubation for a given time, the cells were gathered for measurement of the intrinsic fluorescence of the copolymers used to prepare NPs. The fluorescence was detected using a flow cytometer (Beckman Coulter, USA). Data was analyzed with the CellQuest (Becton Dickinson) software. For measurement of the co-polymers-derived fluorescence, excitation was with the 488 nm line of an argon laser, and emission fluorescence between 564 and 606 nm was measured. For each sample, the data for individual fluorescence of 10,000 cells were collected.

2.9. Subcellular localization of fluorescent NPs

HUVECs and HeLa cells were cultured in NPs-containing DMEM medium (concentration for PMPI-HPAE-co-PLA/DPPE copolymer in various NPs, 250 μg/mL) for 4 h on glass coverslips of 14 mm^2 in culture dishes. To detect the intracellular localization, cells were further incubated with 75 nM LysoTracker Red DND-99 (Invitrogen, Carlsbad, California, USA) for 30 min to label lysosomes. The cells were imaged with a laser confocal scanning microscope (Nikon) equipped with a 60× oil immersion lens. The excitation/emission wavelengths were 488 nm/577 nm for the copolymers and 488 nm/510 nm for LysoTracker.

2.10. Statistical analysis

Results were presented as mean or mean ± standard deviation (SD) (number of experiments). One-way analysis of variance (ANOVA) was applied to evaluate the significance among groups according to the Bonferroni's post-test.

3. Results and discussion

3.1. Synthesis and characterization of dual-targeting and fluorescent copolymers

3.1.1. Synthesis and characterization of fluorescent PMPI-HPAE-co-PLA/DPPE copolymer

The synthetic route of PMPI-HPAE-co-PLA/DPPE copolymer is shown in Supplementary Scheme S1. The molecular weight of the obtained PMPI-HPAE-co-PLA/DPPE copolymer was 50 kDa and polydispersity (M_w/M_n) was 1.51. The final products of PMPI-HPAE-co-PLA/DPPE had good solubility in THF, CHCl$_3$, DMF and DMSO.

Scheme 1. Targeted polymeric NPs can be used to deliver chemotherapeutic drugs to tumor tissues with greater efficacy. (A) The synthetic route for dual-targeting of RGD and Tf conjugation to PMPI-HPAE-co-PLA/DPPE; (B) Schematic illustration of the process of preparing PTX-loaded NPs by a modified emulsion/solvent evaporation method; (C) Schematic representation of the mechanisms by which dual-targeting nanocarrier can deliver PTX to tumor tissues. Passive targeting is achieved by extravasation of NPs through enhanced permeability of the tumor vasculature (EPR effect). Active tumors targeting can be achieved by decoration of RGD and Tf that promote cell-specific recognition and binding. The ligand RGD enhances the targeting migration and accumulation of NPs to the $\alpha_v\beta_3$ integrin-expressing tumor vasculature and Tf then improves the cellular uptake of NPs by TfR-expressing tumor cells.
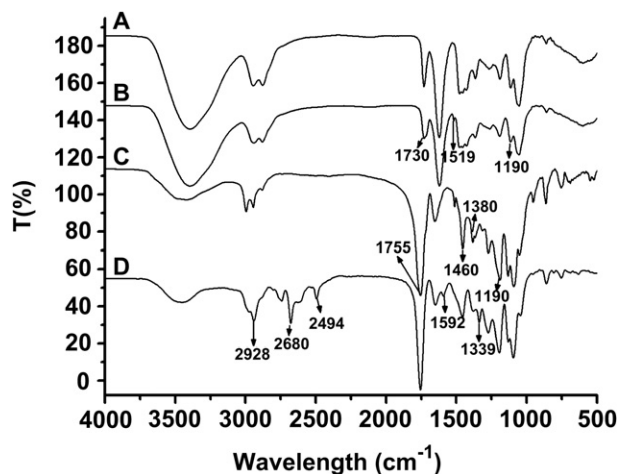
Fig. 1. IR spectra of (A) HPAE-OHs4, (B) PMPI-HPAE, (C) PMPI-HPAE-co-PLA and (D) PMPI-HPAE-co-PLA/DPPE.

Fig. 1 shows the FT-IR spectra of HPAE-OHs4, PMPI-HPAE, PMPI-HPAE-co-PLA and PMPI-HPAE-co-PLA/DPPE, respectively. Compared with the FT-IR spectra of HPAE-OHs4 (Fig. 1A.), the spectrum of PMPI-HPAE (Fig. 1B.) has a new absorption peak at ~ 1519 cm^{-1} (ν_{N-H}), which signified the formation of carbamate linkage between the HPAE-OHs4 and PMPI [24]. In Fig. 1C, the intensity of absorption peaks at 1755 cm^{-1} ($\nu_{C=O}$), 1460 cm^{-1}

(δ_{CH3}), 1380 cm^{-1} (δ_{CH3}), 1190 cm^{-1} (ν_{C-O-C}) became much stronger compared with the corresponding values in Fig. 1B, which suggested the conjugation of PLA to PMPI-HPAE. In Fig. 1D, either the new absorption peaks at 1592 cm^{-1} ($\nu_{O=C-N}$), 2680 cm^{-1} (ν_{P-O}) or the stronger intensity of certain absorption peaks at 1339 cm^{-1} (δ_{CH2}), 2928 cm^{-1} (ν_{CH2}) indicated the successful modification of DPPE to PMPI-HPAE-co-PLA.

The chemical structures of polymers were also confirmed by ^{1}H NMR, ^{13}C NMR and ^{31}P NMR. Fig. 2 exhibits the ^{1}H NMR spectra of HPAE-OHs4, PMPI-HPAE, PMPI-HPAE-co-PLA and PMPI-HPAE-co-PLA/DPPE polymers, respectively. In Fig. 2B, the signal peak at ~ 7.0 ppm attributed to the maleimide protons was detected, which demonstrated the existence of the PMPI on the PMPI-HPAE. Compared with PMPI-HPAE (Fig. 2B), the ^{1}H NMR spectra of PMPI-HPAE-co-PLA copolymer (Fig. 2C) exhibited signals at ~ 1.3 and ~ 1.4 ppm corresponding to the -CH$_3$ protons of the PLA moiety located in the terminal groups and repeat units. The signals at ~ 4.2 and ~ 5.1 ppm were attributed to protons of -CH on the terminal PLA and repeat PLA units in the chain, respectively. These results all verified that the PLA chains were successful introduced to the PMPI-HPAE. The ^{1}H NMR spectrum of PMPI-HPAE-co-PLA/DPPE copolymer (Fig. 2D) showed signals at ~ 8.1 ppm attributed to the -NH protons of the DPPE moiety. All the other signal peaks were assigned to protons of DPPE moiety [33,34]. ^{13}C NMR and ^{31}P NMR spectra confirmed that DPPE was chemically combined with PMPI-HPAE-co-PLA copolymer (Supplementary Figs S1 and S2).

The fluorescence spectra of PMPI-HPAE-co-PLA/DPPE were also explored. Fig. 3A displays the fluorescence emission spectra of
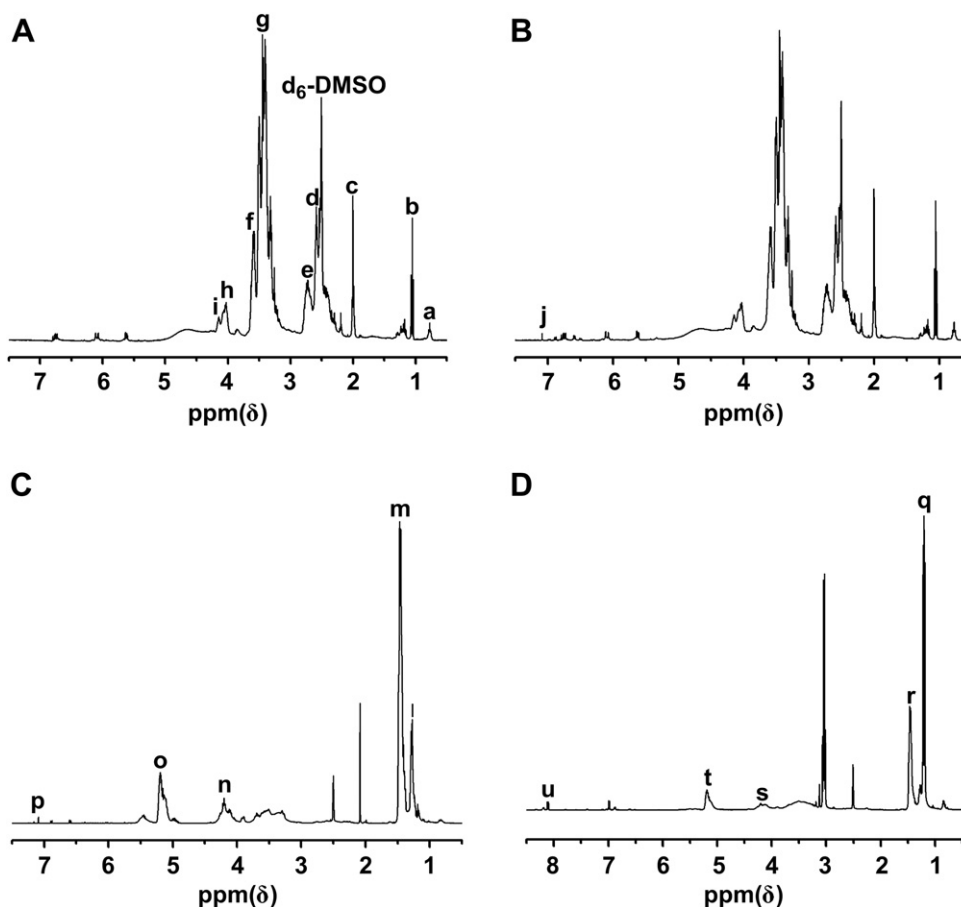

Fig. 2. ^{1}H NMR spectra of (A) HPAE-OHs4, (B) PMPI-HPAE, (C) PMPI-HPAE-co-PLA and (D) PMPI-HPAE-co-PLA/DPPE.
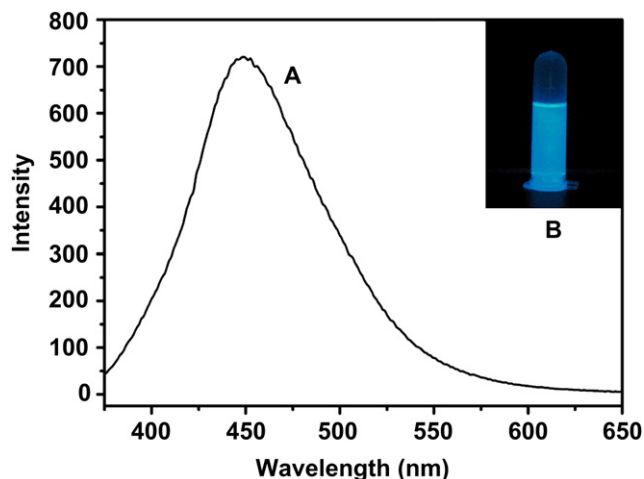
Fig. 3. (A) Fluorescence emission spectrum of PMPI-HPAE-co-PLA/DPPE copolymer (excitation at 367 nm) and (B) An illumination photograph of NPs made by PMPI-HPAE-co-PLA/DPPE in PBS, the solution was excited by a UV lamp at 365 nm.

PMPI-HPAE-co-PLA/DPPE copolymer when excitation band was at 367 nm. The emission band was 452 nm and the quantum yield was 0.51. Fig. 3B shows an illumination photograph of NPs made by PMPI-HPAE-co-PLA/DPPE with an emulsion/solvent method upon UV light excitation. The result dedicated that the intrinsic fluorescence of the polymer was stable and could not be destroyed by organic solvent or sonication. Based on the classic viewpoint, the functional groups in PMPI-HPAE-co-PLA/DPPE could not emit the observed blue fluorescence, so it is not easy to explain the novel fluorescence phenomenon in terms of our present experiments. Nevertheless, HPAE-OHs4 and HPAE-co-PLA were also found to show similar strong fluorescence. Thus the photoluminescence may be attributed to the special backbone of the hyperbranched HPAE-OHs4 polymer [35].

3.1.2. Synthesis of dual-targeting copolymers

The synthetic route of the targeting copolymers is exhibited in Scheme 1A. The RGD-SH and Tf-SH were conjugated to the distal end of HPAE-OHs4 through reaction between sulfhydryl and maleimide groups. This reaction between thiol groups and maleimide is rapid and proceeds close to completion [36,37]. It occurs at nearly neutral pH, at ambient temperature, and even when rather low concentrations of the reactants are present.

An HPLC method was used to detect the binding efficiency of the RGD to the PMPI-HPAE-co-PLA/DPPE copolymer and the result showed that nearly all the RGD was conjugated to the copolymers (see Supplementary Fig. S3). For the determination A bicinchoninic acid (BCA) protein assay with pure holo-transferrin as standard was applied for the determination of the average amount of Tf that conjugated to the copolymers [38]. The calculated coupling efficiency was 1 mg Tf/10 mg polymers.

3.2. Physicochemical characterization of PTX-loaded NPs

An emulsion/solvent evaporation technology was adopted to make PTX-loaded NPs. The NPs were lyophilized for long-time storage and subsequently resuspended in various solvents according to specific applications.

The morphology of PTX-NPs, PTX-Tf-NPs, PTX-RGD-NPs and PTX-RGD/Tf-NPs was observed using TEM (Fig. 4). The NPs appeared to be typical spheres in shape with good dispersion. The average hydrodynamic diameter and surface charge of the obtained

NPs in PBS, determined with DLS, are shown in Table 1. The average size of PTX-NPs was 247.2 nm, while the average size of PTX-Tf-NPs, PTX-RGD-NPs and PTX-RGD/Tf-NPs was slightly enhanced (264.5, 255.4 nm and 259.5 nm, respectively) attributing to the introduction of Tf and RGD [39]. All the NPs showed a narrow size distribution (PDI < 0.3). The zeta potential for the PTX-NPs, PTX-RGD-NPs, PTX-Tf-NPs and PTX-RGD/Tf-NPs was −5.22 mV, −4.35 mV, −10.58 mV and −8.47 mV, respectively. Tf is an anionic protein so that the zeta potential of Tf conjugated NPs was slightly more negative than that without Tf (shown in Table 1) [40]. In addition, the encapsulation efficiency of PTX-NPs, PTX-RGD-NPs, PTX-Tf-NPs and PTX-RGD/Tf-NPs was similar of about 50%, which was almost not affected by the decoration of RGD and Tf.

3.3. Effects of dispersion solutions on the NPs properties

It is important that NPs must be well-dispersed to make sure uniform dosing before in vitro and in vivo studies. Thus, three commonly used solvents (deionized water, PBS of pH 7.4 and DMEM with 10% FBS) were chosen to re-dissolve the dried NPs. As shown in Supplementary Table S1, NPs dispersed in DMEM with 10% FBS exhibited smaller average size and narrower PDI, which may attribute to the stabilizing effect of FBS. No aggregation was observed in the dispersion solutions, which is important for following both in vitro and in vivo researches.

3.4. The influences of formulation parameters on drug loading content and encapsulation efficiency

Loading content and encapsulation efficiency of NPs are two important factors to be considered for researches in vitro or in vivo. Therefore, the influence of different formulation parameters on drug loading content and encapsulation efficiency were investigated in this study. Previous studies showed that the concentration of the emulsifier and the copolymer/drug ratio play vital roles in determining the drug loading content and encapsulation efficiency [41,42]. Therefore, the effects of PVA on drug loading content and encapsulation efficiency were investigated under different copolymer/drug ratios. As shown in Table 2, drug loading content and encapsulation efficiency were investigated under 0.5%, 1% and 2% of PVA. 1% PVA was the optimal condition (with drug loading content 5.14% at a copolymer/PTX ratio of 10/1) when compared with the 0.5% and 2% PVA. Keeping the concentration of PVA constant at 1%, drug loading content and encapsulation efficiency of NPs prepared with different copolymer/drug ratios were analyzed. As the ratio of copolymer/drug increased, the drug loading content decreased while the encapsulation efficiency gradually rose. In addition, the size of NPs at copolymer/PTX ratio of 5/1, 1% PVA was higher than that with the ratio of 10/1 (data not shown). Thus, 10/1 of the mass ratio of copolymer/drug and 1% PVA was selected for further investigation.

3.5. In vitro drug release studies

Controlled and sustained drug release is a desirable feature that we aim to achieve with drug-loaded NPs. The pH value in tumor tissues is much lower than that in the normal tissues owing to excess lactic acid produced by hypoxia and acidic intracellular organelles [43,44], therefore, the drug release profile was performed under a simulated physiological condition (pH 7.4) and in an acidic environment (pH 5.2) at 37 °C in order to assess the feasibility of using PMPI-HPAE-co-PLA/DPPE as an anti-cancer drug delivery carrier. As shown in Fig. 5, the PTX-NPs, PTX-Tf-NPs, PTX-RGD-NPs and PTX-RGD/Tf-NPs all exhibited a sustained drug
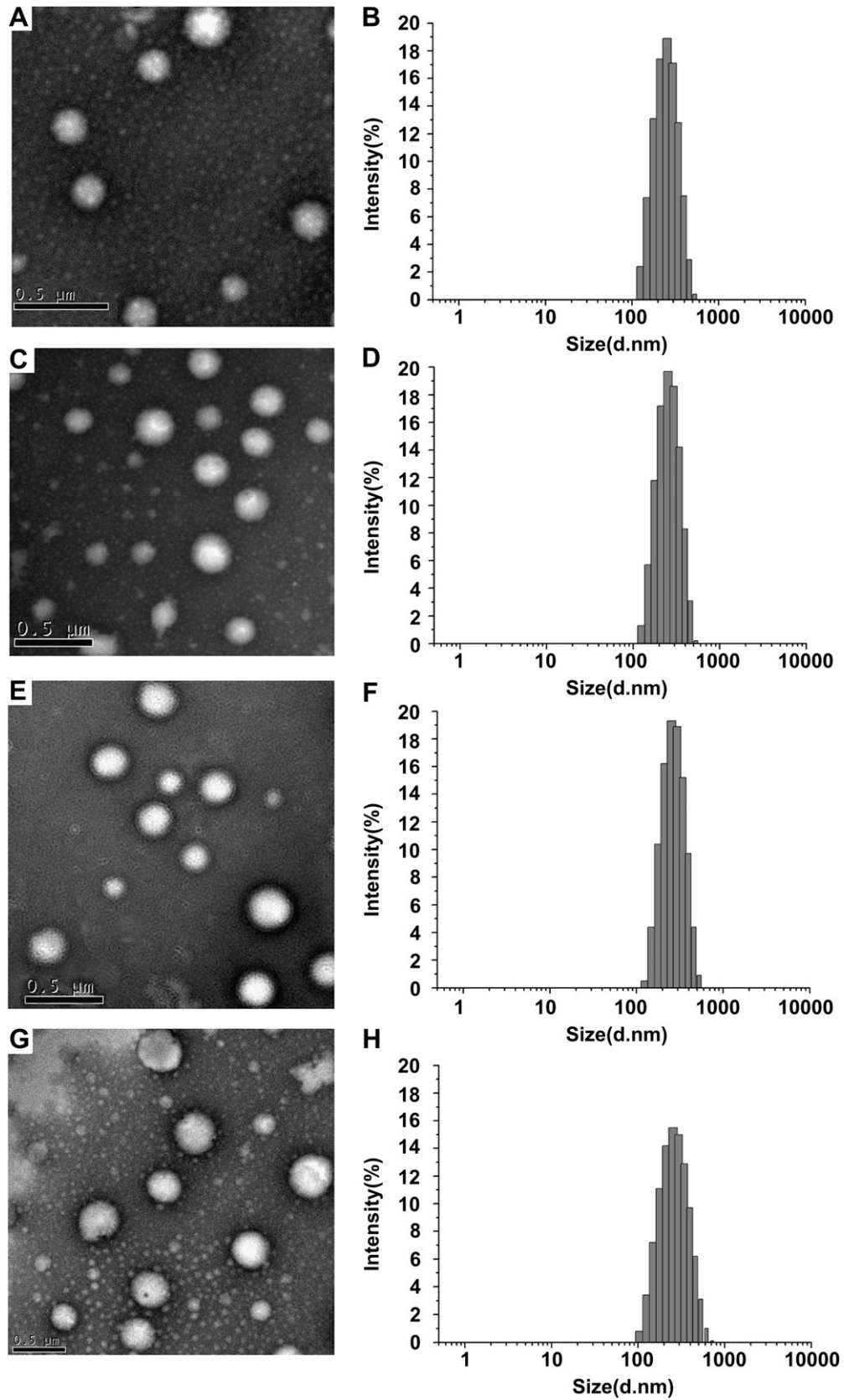
Fig. 4. TEM and DLS characterization of PTX-loaded NPs in PBS. TEM image of (A) PTX-NPs (C) PTX-RGD-NPs (E) PTX-Tf-NPs (G) PTX-RGD-Tf-NPs; DLS histogram of (B) PTX-NPs (D) PTX-RGD-NPs (F) PTX-Tf-NPs (H) PTX-RGD-Tf-NPs. Scale bar for TEM images: 0.5 μm.

Table 1
Physicochemical characteristics of the various PTX-loaded NPs ($n = 3$).

	PTX-NPs	PTX-RGD-NPs	PTX-Tf-NPs	PTX-RGD/Tf-NPs
PTX encapsulation efficiency (%)	51.4 ± 2.1	50.2 ± 3.6	48.8 ± 1.9	50.9 ± 2.5
PTX loading content (%)	5.14 ± 0.06	5.02 ± 0.11	4.88 ± 0.09	5.09 ± 0.08
Size (nm)	247.2 ± 1.5	255.4 ± 1.2	264.5 ± 2.5	259.5 ± 2.8
PDI	0.064 ± 0.01	0.047 ± 0.01	0.174 ± 0.04	0.151 ± 0.03
Zeta potential (mV)	-5.22 ± 1.2	-4.35 ± 1.8	-10.58 ± 1.4	-8.47 ± 2.8

release profiles with total PTX releases from NPs at pH 7.4 of about 50.4%, 40%, 48.7% and 43%, respectively. Meanwhile, drug release profiles at pH 5.2 were also controlled and sustained with total PTX released from NPs of 71%, 65%, 69.6% and 67%, respectively, which were much faster than at pH 7.4. All the NPs had similar drug release profiles. These results were in agreement with previous studies explaining that phosphatidylethanolamine is pH-sensitive that can trigger and enhance drug release [45,46]. The PTX is released slowly at pH 7.4, hence, most of the PTX molecules are still encapsulated in the NPs during the blood circulation, which results in reduced systemic toxicity. Furthermore, the pH sensitivity of the NPs indicates that a faster drug release may take place in acidic tumor environment and intracellular organelles, which would be helpful for tumor therapy.

3.6. Inhibitory effect against tumor cell by PTX-loaded NPs

In our study, cRGDfK and Tf, specific for $\alpha_v\beta_3$ integrin receptors and TfR, respectively, were chosen as the targeting ligands. Previous studies have shown that the HUVECs express a large number of $\alpha_v\beta_3$ integrin receptors, while some tumor cell lines, such as HeLa cells and MCF-7 cells, just express very few or no $\alpha_v\beta_3$ integrin receptors [47,48]. On the contrary, the expression level of TfR on tumor cell lines is much more than on normal cells [15,49]. Therefore, HUVECs and HeLa cells were used to assess the efficacy of the targeting ligands.

Fig. 6 shows the in vitro viability of HUVECs and HeLa cells after 24 h (A and C), 48 h (B and D) culture with free-PTX, PTX-NPs, PTX-RGD-NPs, PTX-Tf-NPs and PTX-RGD/Tf-NPs at the PTX concentration of 0.001–10 μg/mL. Obviously, the cell viability of both cell lines decreased with increasing the incubation time as well as the PTX concentration. The PTX-RGD/Tf-NPs and PTX-RGD-NPs exhibited higher toxicity to HUVECs after incubation for 24 h and 48 h than free PTX and other two loaded NPs (Fig. 6A and B). All the PTX-loaded NPs showed similar cytotoxic effects, but much higher

Table 2
The influences of formulation parameters on drug loading content and encapsulation efficiency ($n = 3$).

| Co-Polymer/PTX mass ratio		5/1	10/1	50/1	100/1
0.5% PVA	Loading content (%)	5.16 ± 0.08	4.32 ± 0.04	0.90 ± 0.02	0.50 ± 0.06
	Encapsulation efficiency (%)	25.8 ± 1.04	43.2 ± 1.66	44.9 ± 0.89	50.3 ± 2.96
1% PVA	Loading content (%)	7.82 ± 0.16	5.14 ± 0.06	1.09 ± 0.02	0.65 ± 0.04
	Encapsulation efficiency (%)	39.1 ± 2.13	51.4 ± 2.10	54.7 ± 0.89	65.3 ± 2.32
2% PVA	Loading content (%)	6.24 ± 0.06	4.27 ± 0.23	0.97 ± 0.05	0.60 ± 0.14
	Encapsulation efficiency (%)	31.2 ± 0.74	42.7 ± 2.75	48.6 ± 1.97	60.1 ± 3.45
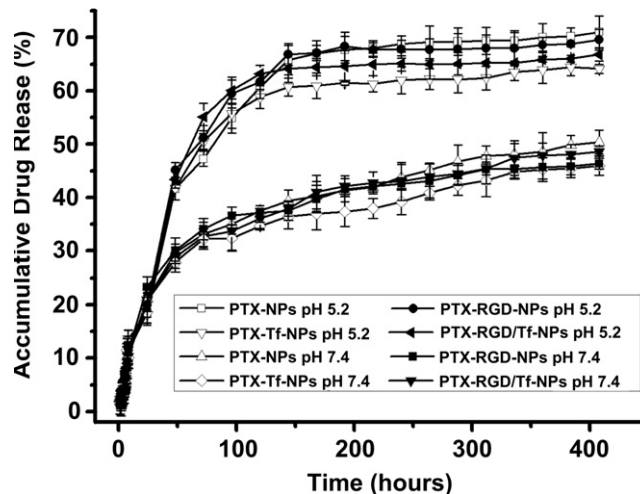
Fig. 5. In vitro drug release profiles of PTX from various PTX-loaded NPs in PBS at pH 5.2 and pH 7.4, respectively, at 37 °C.

than free PTX at 24 h (Fig. 6C). However, at 48 h the PTX-Tf-NPs and PTX-RGD/Tf-NPs could inhibit the growth of tumor cells more efficiently if compared with the other three (Fig. 6D).

The in vitro cytotoxicity and targeting effects of the multifarious formulations of drugs can be quantitatively compared by IC50, the drug concentration at which 50% of cells have been killed, at a predetermined cell culture time. The IC50 values of PTX obtained in different formulations at 48 h are given in Table 3. For HUVECs cells, the PTX-RGD-NPs and PTX-RGD/Tf-NPs formulations had a much lower IC50 (0.05 μg/mL and 0.17 μg/mL, respectively) than the free-PTX, PTX-NPs and PTX-Tf-NPs (0.38 μg/mL, 0.56 μg/mL and 0.37 μg/mL, respectively). Nevertheless, for HeLa cells, the IC50 of PTX-Tf-NPs and PTX-RGD/Tf-NPs (0.22 μg/mL and 0.24 μg/mL) were lower in comparison to free-PTX (0.94 μg/mL), PTX-NPs (0.60 μg/mL) and PTX-RGD-NPs (0.49 μg/mL). Obviously, PTX-RGD-NPs only modified by RGDfK showed stronger cell toxicity to HUVECs, which express abundant $\alpha_v\beta_3$ integrin receptors but few TfR, while PTX-Tf-NPs conjugated with Tf were more toxic to HeLa cells which are rich in TfR but lack of $\alpha_v\beta_3$ integrin. As expected, PTX-RGD/Tf-NPs linked with both RGDfK and Tf ligands exhibited higher cytotoxicity to both cells. Thus, the RGDfK and Tf ligands did play roles in in vitro cytotoxicity and targeting effects. The results would be further verified later in the cell uptake section. Moreover, the PTX formulated in NPs was more effective that free PTX in HeLa cells and this enhanced cytotoxicity may be attributed to DPPE segment on the copolymers, which perhaps increase the endocytosis as it has a similar structure with phospholipids composing the plasma membranes. The blank NPs did not show obvious cytotoxicity up to 250 μg/mL (data not shown).

3.7. Improved uptake efficiency by targeting ligands

One of the advantages of the copolymers is their intrinsic fluorescence that enables the various PTX formulations to be detected directly in order to quantify their cellular uptake and intracellular trafficking. We used fluorescence microscopy to measure the fluorescence intensity of HPAE-co-PLA/DPPE-Tf, HPAE-co-PLA/DPPE-RGD, HPAE-co-PLA/DPPE-Tf-RGD copolymers, the results showed that the conjugation of RGDfK and Tf had no effect on the fluorescence intensity of the polymers (data not shown).

Fig. 7 shows the cellular uptake of PTX-loaded NPs with or without RGDfK and Tf modification. The RGD and Tf modification significantly enhanced the cellular uptake by HUVECs and HeLa
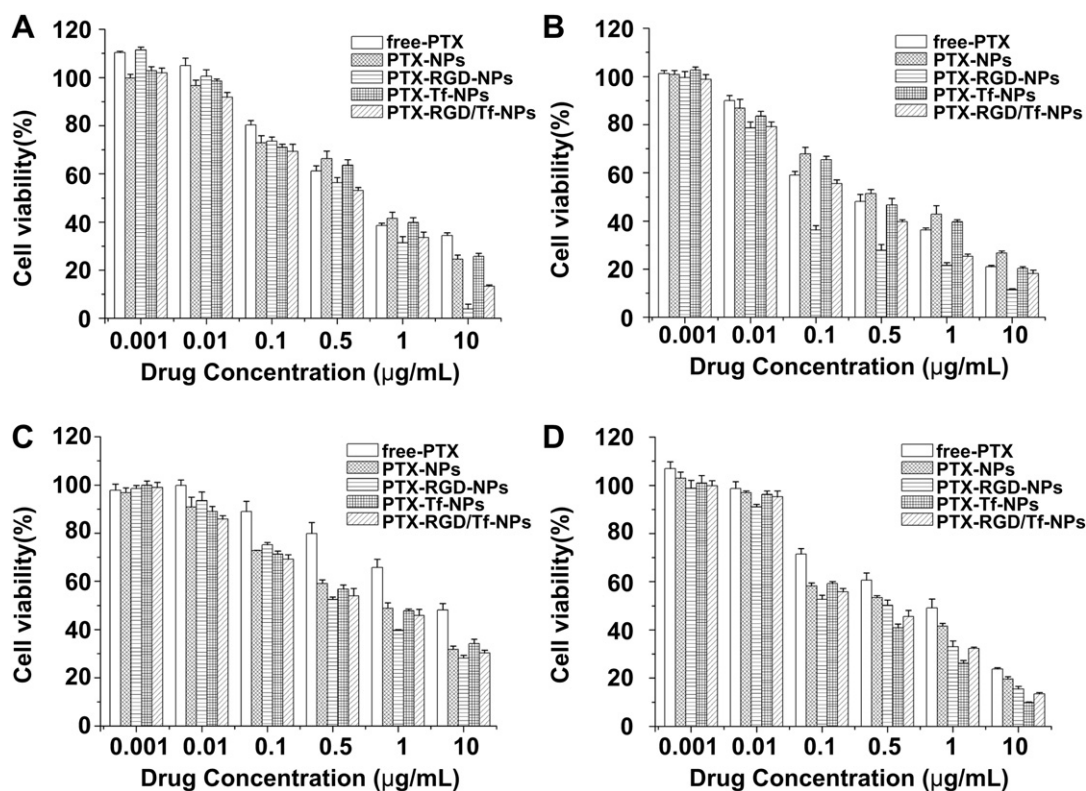
Fig. 6. *In vitro* viability of HUVECs (A, B) and HeLa cells(C, D) treated with different PTX formulations at 0.001, 0.01, 0.1, 0,5, 1, 10 μg/mL drug concentration after 24 h (A,C), 48 h (B,D) incubation, respectively (*n* = 4). Cell viability was determined using the CCK-8 Kits and the absorbance was detected at 450 nm.

cells, respectively. After treatment for 4 h, the cellular uptake of PTX-RGD-NPs only decorated by RGD was 1.6-fold higher (by HUVECs) or no obvious higher (by HeLa cells) than that of PTX-NPs. In case of PTX-Tf-NPs, the cellular uptake by HUVECs was almost the same with PTX-NPs, while 1.34-fold higher by HeLa cells. Furthermore, for PTX-RGD/Tf-NPs modified by the two ligands, it showed 1.7-fold and 1.4-fold greater uptake by HUVECs and HeLa cells compared with PTX-NPs. In addition, the amount of cellular uptake increased with the incubation time. This time-dependent behavior could be explained by the presence of active endocytosis process within the system.

The above cellular uptake and cytotoxicity studies show that PTX-loaded PMPI-HPAE-co-PLA/DPPE copolymers modified with dual-targeting had a faster and greater cellular uptake when compared to PTX-loaded PMPI-HPAE-co-PLA/DPPE copolymers, resulting in enhanced cytotoxicity against HUVECs and HeLa tumor cells.

3.8. Endocytosis and subcellular localization of fluorescent NPs

Cellular uptake and distribution of PTX-loaded NPs in HUVECs and HeLa cells were further detected using laser confocal scanning microscopy. To better compare cell internalization among the various NPs formulations with the help of intrinsic fluorescence of NPs, the images were taken by harmonizing the parameters such as laser power, sensitivity, offset, and gain constant during the cell imaging procedure. Fig. 8A showed that the higher fluorescence intensity was observed in HUVECs treated with PTX-RGD-NPs or PTX-RGD/Tf-NPs compared to those treated with PTX-NPs or PTX-Tf-NPs. In HeLa cells (Fig. 8B), the fluorescence was slightly stronger when cells were incubated with PTX-Tf-NPs or PTX-RGD/Tf-NPs other than PTX-NPs or PTX-RGD-NPs. Therefore, RGDfK-coupled and Tf-coupled NPs showed stronger fluorescence in HUVECs and HeLa cells, respectively, which confirmed the quantitative measurements of cellular uptake of various PTX formulations.

To further investigate the effects of RGDfK and Tf modification on intracellular localization of NPs, their subcellular location are shown in Fig. 9. When HUVECs were treated with PTX-NPs and PTX-RGD-NPs, the merge images in Fig. 9A and B exhibited that most of the two NPs were localized in lysosomes inside the cells; however, when treated with PTX-RGD-NPs, though majority of NPs located in lysosomes, there were part of NPs still stayed on the plasma membranes after incubation for 4 h at 250 μg/mL. The different intracellular distribution between the NPs decorated RGD or not can be explained by their distinct uptake mechanisms. NPs with

Table 3
IC50 values of different PTX formulations after 48 h incubation with HUVECs and HeLa cells (*n* = 4).

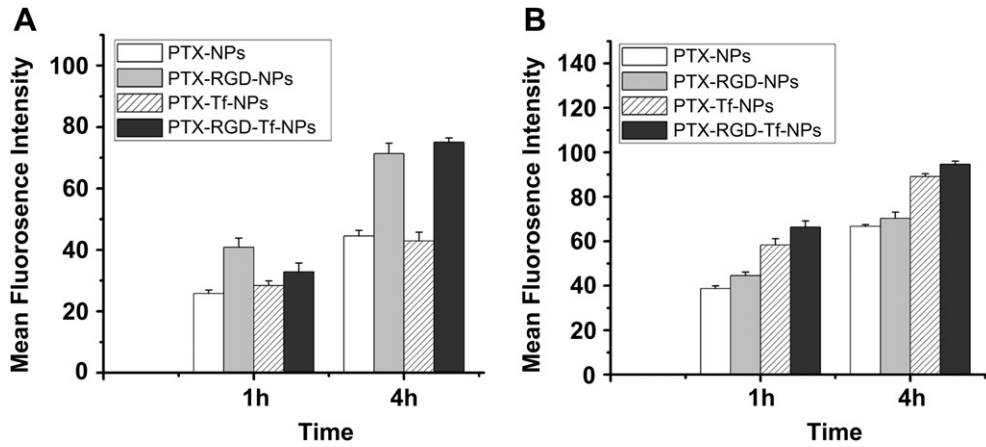| PTX formulation		Free-PTX	PTX-NPs	PTX-RGD-NPs	PTX-Tf-NPs	PTX-RGD/Tf-NPs
IC50 (μg/mL)	HUVECs	0.38 ± 0.014	0.56 ± 0.047	0.05 ± 0.021	0.37 ± 0.033	0.17 ± 0.012
	HeLa cells	0.96 ± 0.031	0.60 ± 0.028	0. 49 ± 0.015	0.22 ± 0.017	0.24 ± 0.023

Fig. 7. The cellular uptake of different PTX formulations in HUVECs (A) and HeLa cells (B) at 250 μg/mL after 1 h and 4 h incubation expressed as geometric mean fluorescence intensity ($n = 3$).
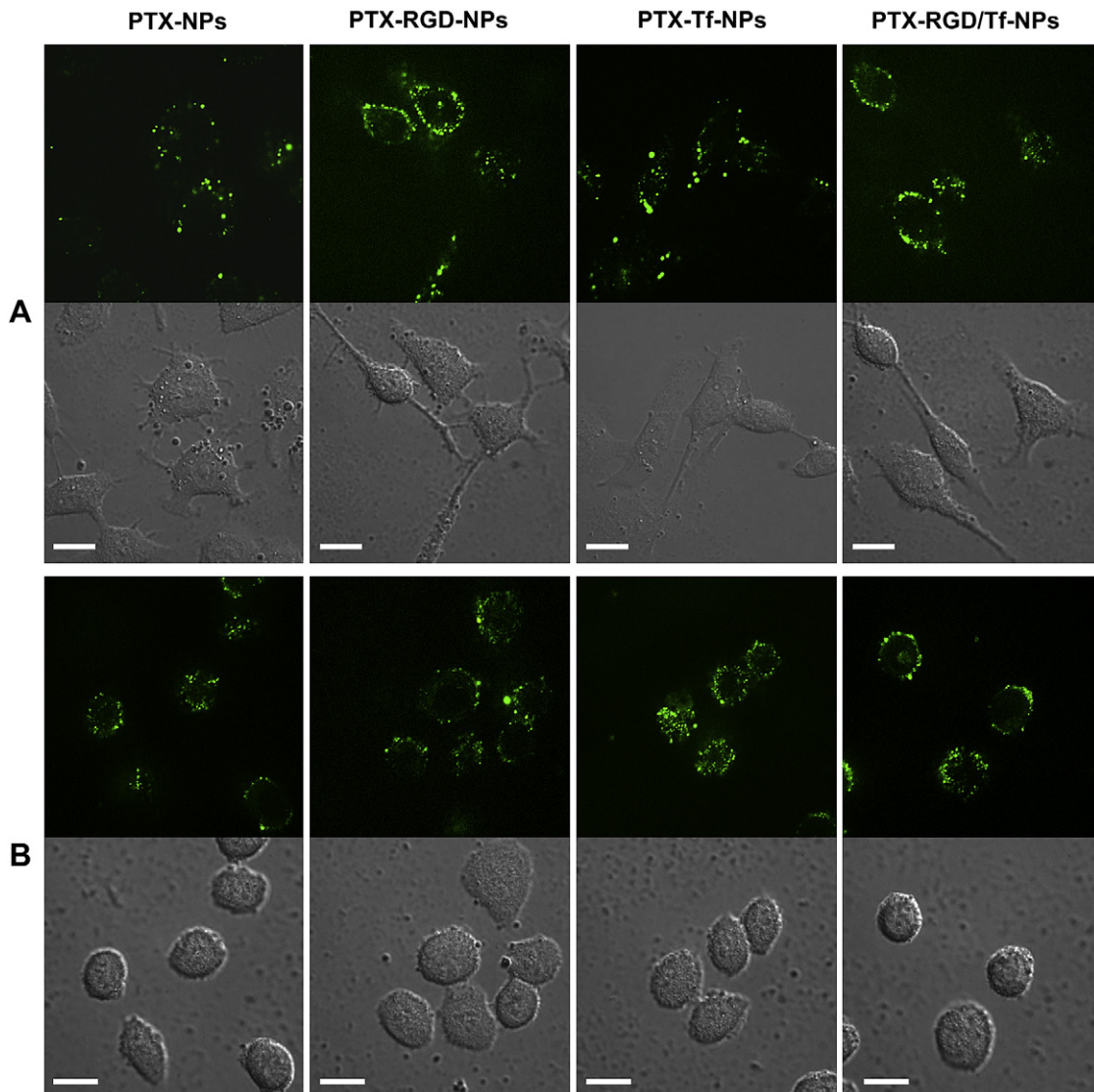

Fig. 8. Intracellular delivery of various PTX formulations in HUVECs (A) and HeLa cells (B). Cells were incubated with PTX-NPs, PTX-RGD-NPs, PTX-Tf-NPs and PTX-RGD/Tf-NPs at the same concentration of 250 μg NPs/mL for 4 h and then detected by confocal microscopy. Scale bar = 20 μm.
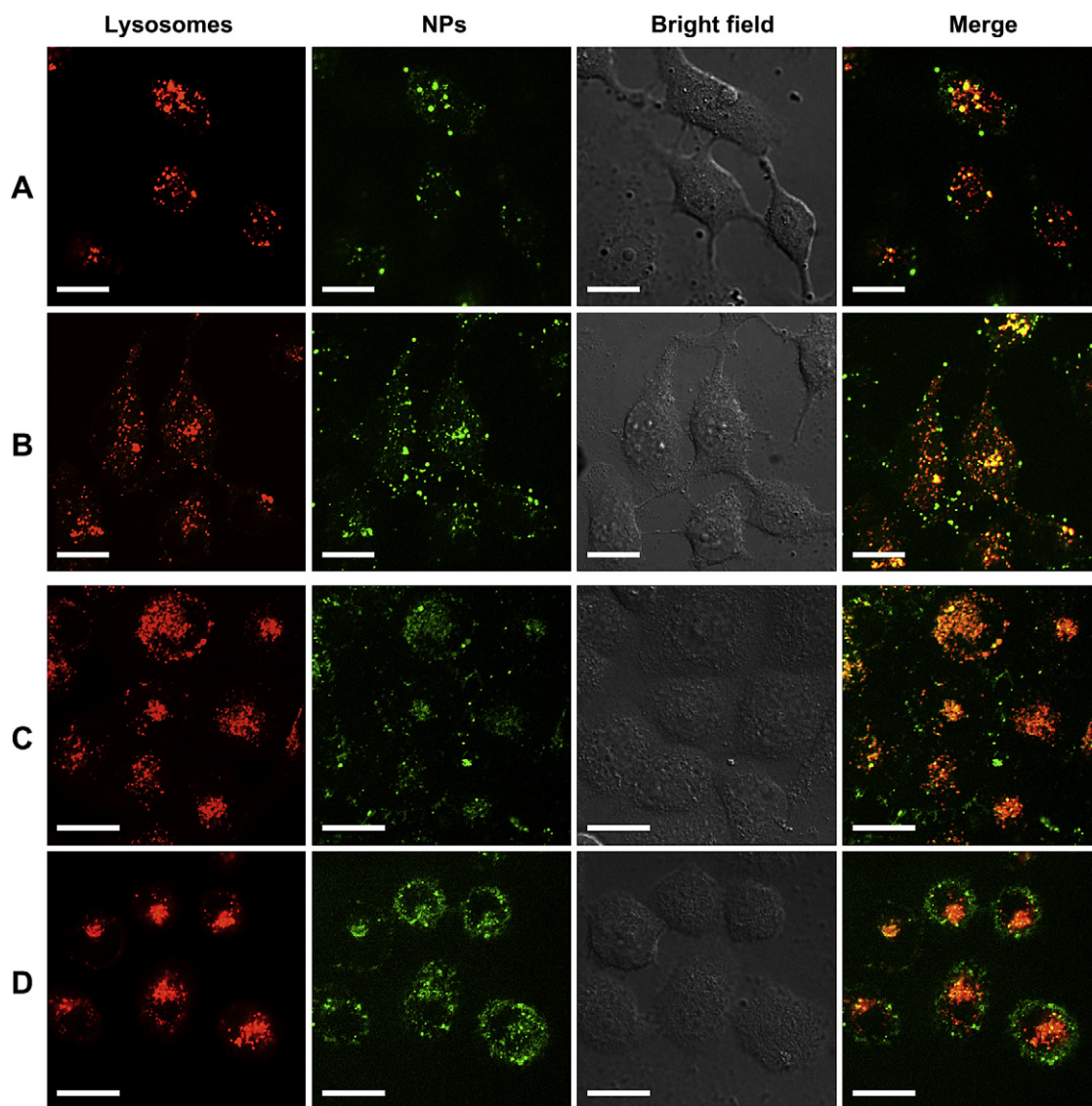
Lysosomes	NPs	Bright field	Merge

Fig. 9. Intracellular localization of different PTX formulations in HUVECs (A,B) and HeLa cells (C,D). Cells were incubated with different PTX formulations at the same concentration of 250 μg PMPI-HPAE-co-PLA copolymer/mL for 4 h at 37 °C, after that treated with LysoTracker Red DND-99 for 30 min and then observed by confocal microscopy. (A) and (B) respectively indicated the distribution of PTX-NPs and PTX-RGD-NPs (green) in HUVECs with labeled lysosomes (red). (C) and (D) respectively indicated the localization of PTX-NPs and PTX-Tf-NPs (green) in HeLa cells with labeled lysosomes (red). Scale bar = 20 μm. (For interpretation of the references to color in this figure legend, the reader is referred to the web version of this article.)

diameters around 200 nm may be absorbed by cells through clathrin- or caveolae-mediated endocytosis [50], while RGD-modified NPs could be internalized into cells by integrin-mediated endocytosis [51]. In addition, more PTX-RG-NPs were swallowed by HUVECs compared with PTX-NPs after incubation for 4 h.

Similarly, when HeLa cells were incubated with PTX-NPs and PTX-Tf-NPs (Fig. 9C and D), most of the two NPs dwelled in lysosomes; But the green circles around HeLa cells in merge image of Fig. 9D indicated certain PTX-Tf-NPs bound on cell surface. This different cell attachment and internalization also attributed to different endocytosis mechanisms between PTX-NPs and PTX-Tf-NPs. Tf decorated NPs could be transported into cell by a specific ligand–receptor interaction other than simply non-specific absorption depending on the size [52].

To confirm the different endocytic pathways among various NPs, Fig. 10 shows the dynamic cellular uptake process of PTX-NPs (A) and PTX-Tf-NPs (B) by HeLa cells at different time points. Fig. 10A exhibited that PTX-NPs entered into the cells rapidly after

incubation for 30 min and the amount increased with the incubation time in agreement with the result in Fig. 7. In contrast, PTX-Tf-NPs in Fig. 10B showed a delayed endocytosis process compared with PTX-NPs. A large amount of PTX-Tf-NPs accumulated on the plasma membranes during the first 30 min and then gradually entered inside the cells. Obvious attachment on the cell membrane for longer time should be attributed to the specific transferrin/transferrin receptor-mediated endocytosis [53]. The conjugation of Tf and the TfR extended the time of NPs on the cell membrane. However, most of NPs accumulated in lysosome after incubation for 12 h, regardless of containing Tf or not. According to the result of *in vitro* drug release, a faster drug release occurs when the NPs internalized into the cells from the external neutral environment, leading to a desirable pH-dependent controlled release in lysosomes.

Overall, our data showed the feasibility of using the PMPI-HPAE-co-PLA/DPPE copolymer for delivery of drugs into cells and demonstrated higher anti-tumor efficacy *in vitro*. Thus, it can be
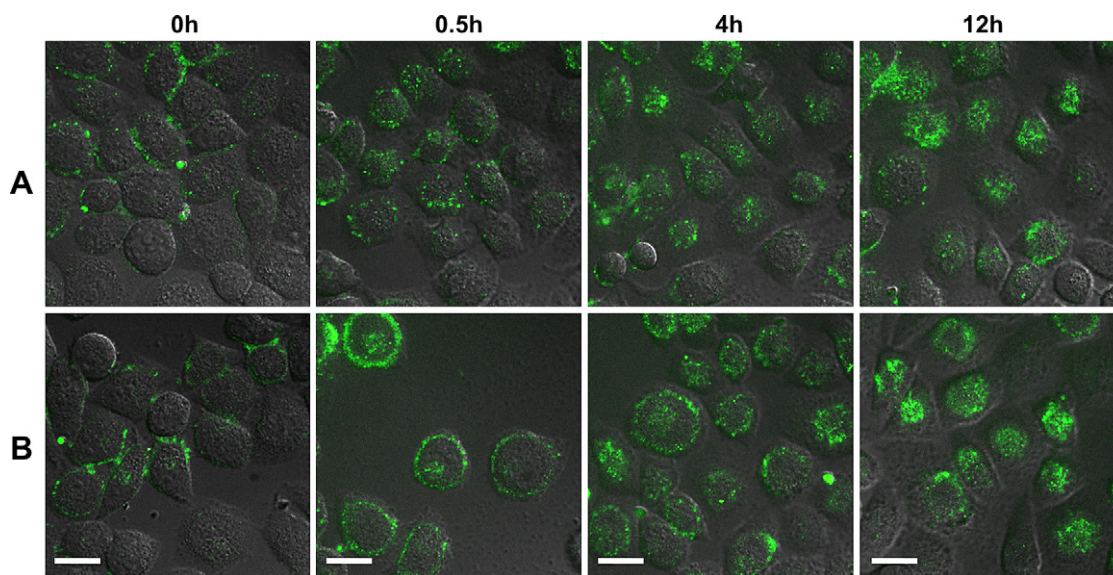
Fig. 10. Time course of intracellular delivery of PTX-loaded NPs in HeLa cells. Cells were incubated with PTX-NPs (A) and PTX-Tf-NPs (B) at the same concentration of 250 μg PMPI-HPAE-co-PLA copolymer/mL for various time points at 37 °C, and then observed by confocal microscopy. Scale bar = 20 μm.

predicted that if the PTX-loaded dual-targeting NPs are applied *in vivo* experiments, the ligands RGD and Tf would enhance the targeting migration and accumulation of NPs to tumor tissues. However, the *in vivo* experiments in tumor-bearing models will be tested in the near future.

4. Conclusions

Dual-targeting PTX-loaded NPs modified with RGDfK and Tf have been successfully constructed with satisfactory size distribution, high encapsulated efficiency and a pH-dependent release profile. Modification of RGDfK and Tf triggered specific ligand–receptor interaction and further led to enhanced intracellular uptake of the PTX-loaded NPs, which explained the enhanced anti-tumor efficiency of dual-targeting PTX-loaded NPs *in vitro*. The observed advantages of PTX-loaded NPs justify future studies in targeted tumor therapies. Therefore, the present formulation of NPs decorated with targeting ligands shows substantial promise for the targeting drug delivery and effective chemotherapeutics.

Appendix. Supplementary material

Supplementary data associated with this article can be found, in the online version, at doi:10.1016/j.biomaterials.2011.11.012.

References

[1] Singla AK, Garg A, Aggarwal D. Paclitaxel and its formulations. Int J Pharmaceut 2002;235:179–92.
[2] Schiff PB, Fant J, Horwitz SB. Promotion of microtubule assembly in vitro by taxol. Nature 1979;277:665–7.
[3] Gelderblom H, Verweij J, Nooter K, Sparreboom A, Cremophor EL. the drawbacks and advantages of vehicle selection for drug formulation. Eur J Cancer 2001;37:1590–8.
[4] Woodle MC. Controlling liposome blood clearance by surface-grafted polymers. Adv Drug Deliver Rev 1998;32:139–52.
[5] Maeda H, Wu J, Sawa T, Matsumura Y, Hori K. Tumor vascular permeability and the EPR effect in macromolecular therapeutics: a review. J Control Release 2000;65:271–84.
[6] Byrne JD, Betancourt T, Brannon-Peppas L. Active targeting schemes for nanoparticle systems in cancer therapeutics. Adv Drug Deliver Rev 2008;60: 1615–26.
[7] Barczyk M, Carracedo S, Gullberg D. Integrins. Cell Tissue Res 2010;339: 269–80.
[8] Hynes RO. A reevaluation of integrins as regulators of angiogenesis. Nat Med 2002;8:918–21.
[9] Murphy EA, Majeti BK, Barnes LA, Makale M, Weis SM, Lutu-Fuga K, et al. Nanoparticle-mediated drug delivery to tumor vasculature suppresses metastasis. P Natl Acad Sci USA 2008;105:9343.
[10] Brooks PC, Clark R, Cheresh DA. Requirement of vascular integrin alpha v beta 3 for angiogenesis. Science 1994;264:569.
[11] Schiffelers RM, Koning GA, ten Hagen TLM, Fens M, Schraa AJ, Janssen A, et al. Anti-tumor efficacy of tumor vasculature-targeted liposomal doxorubicin. J Control Release 2003;91:115–22.
[12] Temming K, Schiffelers RM, Molema G, Kok RJ. RGD-based strategies for selective delivery of therapeutics and imaging agents to the tumour vasculature. Drug Resist Update 2005;8:381–402.
[13] Ponka P, Lok CN. The transferrin receptor: role in health and disease. Int J Biochem Cell B 1999;31:1111–37.
[14] Cazzola M, Bergamaschi G, Dezza L, Arosio P. Manipulations of cellular iron metabolism for modulating normal and malignant cell proliferation: achievements and prospects. Blood 1990;75:1903–19.
[15] Yoon DJ, Chu DSH, Ng CW, Pham EA, Mason AB, Hudson DM, et al. Genetically engineering transferrin to improve its in vitro ability to deliver cytotoxins. J Control Release 2009;133:178–84.
[16] Gan CW, Feng SS. Transferrin-conjugated nanoparticles of poly(lactide)-D-alpha-tocopheryl polyethylene glycol succinate diblock copolymer for targeted drug delivery across the blood-brain barrier. Biomaterials 2010;31: 7748–57.
[17] Huang RQ, Qu YH, Ke WL, Zhu JH, Pei YY, Jiang C. Efficient gene delivery targeted to the brain using a transferrin-conjugated polyethyleneglycol-modified polyamidoamine dendrimer. FASEB J 2007;21:1117–25.
[18] Chen S, Zhang XZ, Cheng SX, Zhuo RX, Gu ZW. Functionalized amphiphilic hyperbranched polymers for targeted drug delivery. Biomacromolecules 2008;9:2578–85.
[19] Gillies ER, Frechet JMJ. Dendrimers and dendritic polymers in drug delivery. Drug Discov Today 2005;10:35–43.
[20] Wu Y, Jiao F, Han S, Fan T, Liu Y, Li W, et al. Construction of amphiphilic copolymer nanoparticles based on hyperbranched poly (amine-ester) and 1,2-dipalmitoyl-sn-glycero-3-phosphoethanolamine as drug carriers for cancer therapy. Nanomed Nanotechnol Biol Med. doi:10.1016/j.nano.2011.04.010.

[21] Miao QH, Xu DX, Wang Z, Xu L, Wang TW, Wu Y, et al. Amphiphilic hyper-branched co-polymer nanoparticles for the controlled delivery of anti-tumor agents. Biomaterials 2010;31:7364–75.

[22] Soenen SJH, Illyes E, Vercauteren D, Braeckmans K, Majer Z, De Smedt SC, et al. The role of nanoparticle concentration-dependent induction of cellular stress in the internalization of non-toxic cationic magnetoliposomes. Biomaterials 2009;30:6803–13.

[23] Al-Jamal WT, Kostarelos K. Liposome-nanoparticle hybrids for multimodal diagnostic and therapeutic applications. Nanomedicine-UK 2007;2:85–98.

[24] Levesque SG, Shoichet MS. Synthesis of enzyme-degradable, peptide-cross-linked dextran hydrogels. Bioconjug Chem 2007;18:874–85.

[25] Annunziato ME, Patel US, Ranade M, Palumbo PS. p-Maleimidophenyl isocy-anate: a novel heterobifunctional linker for hydroxyl to thiol coupling. Bio-conjug Chem 1993;4:212–8.

[26] Jiang M, Wu Y, He Y, Nie J. Micelles formed by self-assembly of hyperbranched poly (amine-ester)-co-(D, L-lactide) (HPAE-co-PLA) copolymers for protein drug delivery. Polym Int 2009;58:31–9.

[27] Wang T, Zhang C, Liang X-J, Liang W, Wu Y. Hydroxypropyl-β-cyclodextrin copolymers and their nanoparticles as doxorubicin delivery system. J Pharm Sci-US 2011;100:1067–79.

[28] Lu W, Zhang Y, Tan YZ, Hu KL, Jiang XG, Fu SK. Cationic albumin-conjugated pegylated nanoparticles as novel drug carrier for brain delivery. J Control Release 2005;107:428–48.

[29] Ellman GL. Tissue sulfhydryl groups. Arch Biochem Biophys 1959;82:70–7.

[30] Nasongkla N, Shuai X, Ai H, Weinberg BD, Pink J, Boothman DA, et al. cRGD-functionalized polymer micelles for targeted doxorubicin delivery. Angew Chem Int Edit 2004;43:6323–7.

[31] He H, Li Y, Jia XR, Du J, Ying X, Lu WL, et al. PEGylated poly(amidoamine) dendrimer-based dual-targeting carrier for treating brain tumors. Biomate-rials 2011;32:478–87.

[32] Danhier F, Lecouturier N, Vroman B, Jerome C, Marchand-Brynaert J, Feron O, et al. Paclitaxel-loaded PEGylated PLGA-based nanoparticles: in vitro and in vivo evaluation. J Control Release 2009;133:11–7.

[33] Percot A, Briane D, Coudert R, Reynier P, Bouchemal N, Lievre N, et al. Hydroxyethylated cholesterol-based cationic lipid for DNA delivery: effect of conditioning. Int J Pharmaceut 2004;278:143–63.

[34] Lebouc F, Dez I, Madec PJ. NMR study of the phosphonomethylation reaction on chitosan. Polymer 2005;46:319–25.

[35] Wang DJ, Imae T. Fluorescence emission from dendrimers and its pH dependence. J Am Chem Soc 2004;126:13204–5.

[36] Hansen CB, Kao GY, Moase EH, Zalipsky S, Allen TM. Attachment of antibodies to sterically stabilized liposomes: evaluation, comparison and optimization of coupling procedures. BBA-Biomembranes 1995;1239:133–44.

[37] Martin FJ, Papahadjopoulos D. Irreversible coupling of immunoglobulin frag-ments to preformed vesicles. An improved method for liposome targeting. J Biol Chem 1982;257:286.

[38] Derycke ASL, De Witte PAM. Transferrin-mediated targeting of hypericin embedded in sterically stabilized PEG-liposomes. Int J Oncol 2002;20:181–7.

[39] Ying X, Wen H, Lu WL, Du J, Guo J, Tian W, et al. Dual-targeting daunorubicin liposomes improve the therapeutic efficacy of brain glioma in animals. J Control Release 2010;141:183–92.

[40] Bellocq NC, Pun SH, Jensen GS, Davis ME. Transferrin-containing, cyclodextrin polymer-based particles for tumor-targeted gene delivery. Bioconjug Chem 2003;14:1122–32.

[41] Bayomi MA. Aqueous preparation and evaluation of albumin-chitosan microspheres containing indomethacin. Drug Dev Ind Pharm 2004;30: 329–39.

[42] Craparo EF, Cavallaro G, Bondi ML, Giammona G. Preparation of polymeric nanoparticles by photo-crosslinking of an acrylloylated polyaspartamide in w/o microemulsion. Macromol Chem Phys 2004;205:1955–64.

[43] Ko J, Park K, Kim YS, Kim MS, Han JK, Kim K, et al. Tumoral acidic extracellular pH targeting of pH-responsive MPEG-poly (beta-amino ester) block copolymer micelles for cancer therapy. J Control Release 2007;123: 109–15.

[44] Bae Y, Jang WD, Nishiyama N, Fukushima S, Kataoka K. Multifunctional polymeric micelles with folate-mediated cancer cell targeting and pH-triggered drug releasing properties for active intracellular drug delivery. Mol Biosyst 2005;1:242–50.

[45] Connor J, Yatvin MB, Huang L. pH-sensitive liposomes: acid-induced liposome fusion. P Natl Acad Sci USA 1984;81:1715.

[46] Gerasimov OV, Boomer JA, Qualls MM, Thompson DH. Cytosolic drug delivery using pH- and light-sensitive liposomes. Adv Drug Deliver Rev 1999;38: 317–38.

[47] Ogawara KI, Rots MG, Kok RJ, Moorlag HE, van Loenen AM, Meijer DKF, et al. A novel strategy to modify adenovirus tropism and enhance transgene delivery to activated vascular endothelial cells in vitro and in vivo. Hum Gene Ther 2004;15:433–43.

[48] Borgne-Sanchez A, Dupont S, Langonne A, Baux L, Lecoeur H, Chauvier D, et al. Targeted Vpr-derived peptides reach mitochondria to induce apoptosis of alpha(V)beta(3)-expressing endothelial cells. Cell Death Differ 2007;14: 422–35.

[49] Noto JM, Cornelissen CN. Identification of TbpA residues required for transferrin-iron utilization by Neisseria gonorrhoeae. Infect Immun 2008;76: 1960–9.

[50] Rejman J, Oberle V, Zuhorn IS, Hoekstra D. Size-dependent internalization of particles via the pathways of clathrin-and caveolae-mediated endocytosis. Biochem J 2004;377:159–69.

[51] Xiong XB, Huang Y, Lu WL, Zhang X, Zhang H, Nagai T, et al. Intracellular delivery of doxorubicin with RGD-modified sterically stabilized liposomes for an improved antitumor efficacy: in vitro and in vivo. J Pharm Sci-US 2005;94: 1782–93.

[52] Sapra P, Allen TM. Internalizing antibodies are necessary for improved ther-apeutic efficacy of antibody-targeted liposomal drugs. Cancer Res 2002;62: 7190–4.

[53] Li HY, Qian ZM. Transferrin/transferrin receptor-mediated drug delivery. Med Res Rev 2002;22:225–50.